NASA TECHNICAL NOTE

NASA TN D-2411

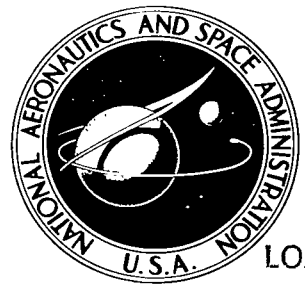

NASA TN D-2411

ANALYSIS OF FULLY DEVELOPED LAMINAR HEAT TRANSFER IN THIN RECTANGULAR CHANNELS WITH HEATING ON THE BROAD WALLS EXCEPT NEAR THE CORNERS

by Joseph M. Savino, Robert Siegel, and Edward C. Bittner

Lewis Research Center
Cleveland, Ohio

NATIONAL AERONAUTICS AND SPACE ADMINISTRATION • WASHINGTON, D. C. • AUGUST 1964

ANALYSIS OF FULLY DEVELOPED LAMINAR HEAT TRANSFER IN THIN RECTANGULAR CHANNELS WITH HEATING ON THE BROAD WALLS EXCEPT NEAR THE CORNERS

By Joseph M. Savino, Robert Siegel, and Edward C. Bittner

Lewis Research Center
Cleveland, Ohio

NATIONAL AERONAUTICS AND SPACE ADMINISTRATION

For sale by the Office of Technical Services, Department of Commerce,
Washington, D.C. 20230 -- Price $0.75

ANALYSIS OF FULLY DEVELOPED LAMINAR HEAT TRANSFER IN THIN RECTANGULAR CHANNELS WITH HEATING ON THE BROAD WALLS EXCEPT NEAR THE CORNERS*

by Joseph M. Savino, Robert Siegel, and Edward C. Bittner

Lewis Research Center

SUMMARY

An analysis is presented of convective heat transfer in thin rectangular channels such as those commonly found in nuclear-reactor fuel assemblies. The velocity and temperature profiles are both assumed to be fully developed. Heating takes place in the fueled region located on the broad channel sides, but the fuel extends only part way to the corners. The short sides and portions of the broad sides that are not fueled are assumed insulated. The wall temperature distributions are shown to be strongly dependent on the spacing between the heated region and the corners. For uniform heating the maximum wall temperature shifts rapidly from the corner to the center of the broad side as this spacing is increased from zero to only one-half the distance between the broad sides. With a cosine heating distribution where the peak flux is at the fuel edges, the wall temperature gradients are more severe than for the uniform heating case. Tables of temperature distributions in the fluid are also given.

INTRODUCTION

Many nuclear reactors utilize assemblies of flat or slightly curved fuel plates. For example, in figure 1 a cross-sectional view is shown of the fuel assembly used in the NASA Plum Brook Reactor. In such an assembly approximately 97 percent of the heat is generated in the fueled portion of the plates and only 3 percent in the unfueled portions and side plates (unpublished Lewis report by K. J. Baumeister and H. J. Reilly). Cooling is accomplished by passing high velocity water, which also serves as the moderator, through the channels between the plates. The local plate-temperature variations are influenced by factors such as local flow velocity, distribution of heat generation over the fueled area, distance from the inlet, heat conduction in the channel wall, and space between the edge of the fuel loading and the corner. A problem of particular concern is the heat transfer in the channel corners. In this region accurate calculations of the wall temperatures are very difficult for several reasons. If the flow is turbulent, the low velocities in the corners may give rise to a larger laminar region than exists in an ordinary laminar sublayer, and the extent of the laminar region is difficult to define.

*Presented at the American Institute of Chemical Engineers Symposium on Nuclear Engineering Heat Transfer, Chicago, Ill., Dec. 1962.

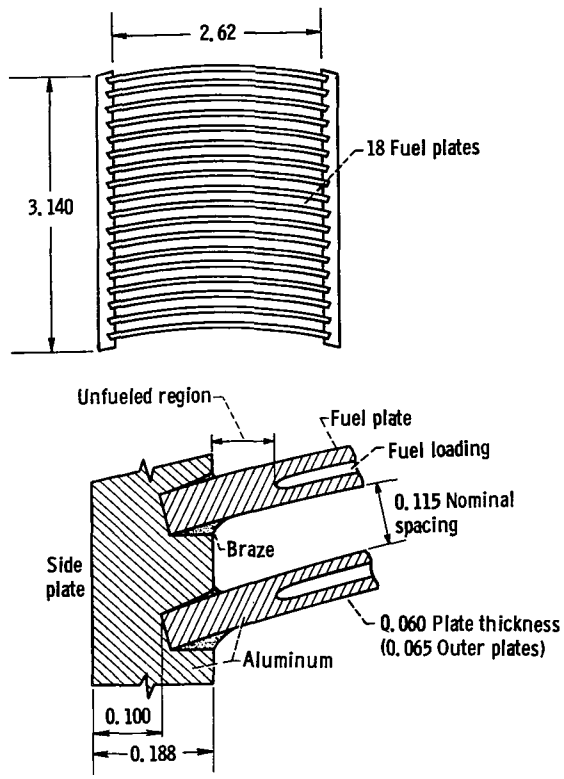

Figure 1. - Cross section of the fuel assemblies used in the NASA Plum Brook Reactor. (All dimensions in inches.)

Away from the walls in the turbulent core, secondary flows exist, and little is known about their influence on the heat transfer. The nominal spacing between the edge of the fuel loading and the corner is variable because of manufacturing tolerance errors. The problem is further complicated by the heat conduction in the fuel plates and in the supporting side walls. Thus, any computations can be at best only approximate.

Convective heat transfer inside noncircular ducts has been studied by a number of investigators, but only the literature that has direct application to the subject of this paper will be mentioned herein. Levy, Fuller, and Niemi (ref. 1) experimentally studied turbulent forced-convection heat transfer and boiling burnout for water flowing through rectangular passages of aspect ratio 20 that were electrically heated on all sides. The wall temperatures at the center of the short sides were considerably higher than those on the broad sides. The corner temperatures were not measured, but they may have been the highest temperatures even with heat conduction present in the walls.

Sparrow and Siegel (ref. 2) used variational methods to analyze laminar heat transfer in a rectangular channel of aspect ratio 10 with uniform heating on either all four sides or on only the two broad sides. In both cases the highest wall temperatures occurred in the corners, and the wall temperature variations resulting from heating on four sides were much greater than the temperature variations for heating on only the two broad sides. A direct analysis for uniform heating on all four sides was carried out by Cheng (ref. 3) and evaluated numerically for aspect ratios from 1 to 4. It is significant to note that the laminar analyses gave wall temperatures that were qualitatively similar to those reported in reference 1 for turbulent flow.

Eckert and Irvine (ref. 4) investigated the flow in channels with isosceles triangular cross sections and found that, when the core was turbulent, laminar flow persisted far from the inlet in the apex angle. They also experimented with the heat transfer inside an electrically heated triangular (isosceles with 11.48° apex angle) duct (ref. 5) and measured apex wall temperatures that were much higher than at the other two corners. In the experiment, the heat conduction in the walls reduced the apex temperature below that which would exist for nonconducting walls. The measured wall temperatures were com-

pared with theoretical values calculated by Eckert, Irvine, and Yen (ref. 6) for laminar heat transfer in the same shape passage with no conduction in the walls. Again the laminar analysis gave wall temperatures that were in qualitative agreement with the measured values of the turbulent flow case. The laminar results, however, predicted wall temperatures that were much greater in the corners.

Baumeister and Reilly studied analytically the heat transfer in the corner of a rectangular reactor cooling passage for several specific cases using typical volume heating rates in the fueled and unfueled sections of the fuel plate and side wall. They took into account conduction in the walls, the variation in the distance between the edge of the fuel loading and the corner, and the quality of the brazed bond between the fuel and side plates. They assumed, however, a constant convective heat-transfer coefficient across each wall surface inside the channel, whereas in reality the coefficient varies in the corner. With this assumption the lowest wall temperature was generally at the corners except for the case of a poorly brazed joint. Results were also calculated for the case of uniform heating in all the walls in order to compare them with the results from reference 1. For the preceding condition the calculated wall temperatures were highest in the corners and were considerably greater than those for the case of heating in only the fueled plates.

This report is concerned with a more detailed study of the influence of the spacing between the edge of the fuel loading and the corners of a flat rectangular duct on the wall temperature distribution. Also included in the analysis is the effect of nonuniform heating in the fueled region, which results from a variation in the neutron flux over the width of the broad sides and from self shielding. The flux is sometimes higher near the channel corners due to the reflection of neutrons from adjacent reflector components. Rectangular ducts are treated with aspect ratios of 10 and 20. The flow is taken to be laminar, and both the flow and heat transfer are assumed to be fully developed. The heat generation takes place only in the fueled portion of the broad sides. The unfueled remainder of the broad sides and the short sides are assumed to be perfectly insulated. The small amounts of gamma and neutron heating that occur in them are neglected. No simplifying assumptions are made with reference to the convective heat-transfer coefficient, which varies around the periphery of the channel. The wall and the local fluid temperatures are computed for various spacings between the edge of the fuel loading and the corners.

SYMBOLS

a half-length of short sides of rectangular duct

b half-length of broad sides of rectangular duct

C Jacobi matrix associated with Ω and its decomposition

c half-length of heated width on broad sides

c_p specific heat of fluid at constant pressure

d	unheated width on broad sides between corner and edge of fuel, b-c
dA	element of area
ds	element of length
k	thermal conductivity of fluid
N	number of increments on side of one-fourth of channel cross section
n	number of increments that are heated, $c/\Delta y$ (except where used as a summation index)
P	amplitude in cosine variation of heat flux
p	static pressure
Q	heat-transfer rate to fluid per unit channel length
q	local wall heat addition per unit area
T	temperature
T_b	bulk fluid temperature
T_w	local wall temperature
u	local fluid velocity
$\bar{u}$	average fluid velocity
V_i	eigenvectors of C
X	dimensionless short-side coordinate, x/a
x	coordinate measured along short side
Δx	distance between nodes in x-direction
Y	dimensionless long-side coordinate, y/b
y	coordinate measured along broad side
Δy	distance between nodes in y-direction
z	coordinate measured along duct length
Δ	dimensionless distance between nodes in both x- and y-directions
γ	aspect ratio of rectangular duct, b/a

θ dimensionless temperature, $\frac{T}{Q/4k}$

θ_b dimensionless bulk temperature

θ_L solution of Laplace equation

θ_P solution of Poisson equation

$\underline{\theta}$ temperature solution of discrete problem

$\underline{\theta}^{(m)}$ m^{th} approximation for $\underline{\theta}$ in iterative solution

λ_i eigenvalues of C

μ absolute viscosity

ν outward directed normal to the boundary

ρ fluid density

ω overrelaxation parameter

ω_b optimum value for ω

ANALYSIS

The flat rectangular duct under consideration is shown in figure 2 along with the coordinate system. The principal assumptions are (1) peripheral heat conduction in the walls is not accounted for; hence, the results are for the limiting case where the walls are nonconducting; (2) fluid properties are constant; (3) both the velocity and temperature distributions are fully developed; and (4) the flow is laminar.

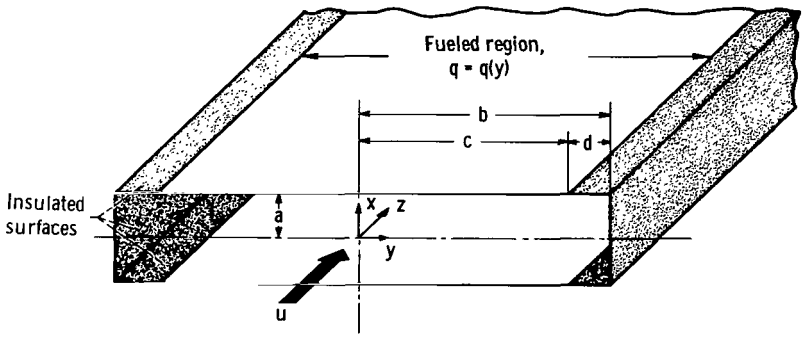

Figure 2. - Coordinate system for thin rectangular channel.

The heat generated in the wall is transferred to the flowing coolant, where it is simultaneously convected downstream and diffused throughout the cross section. The resultant fluid and wall temperature distributions depend on the variation of the coolant velocity over the cross section; hence, the energy equation for the temperature distribution cannot be treated until the velocities are specified. Since the fluid properties are assumed to be independent of temperature, the velocities can be determined before the energy equation is considered.

Velocity Distribution

For steady fully developed laminar flow the momentum equations reduce to a single relation between the pressure gradient in the axial direction and the laminar shear forces:

$$\frac{dp}{dz} = \mu\left(\frac{\partial^2 u}{\partial x^2} + \frac{\partial^2 u}{\partial y^2}\right) \tag{1}$$

The solution for $u(x,y)$ is readily available, for example, in Knudsen and Katz (ref. 7), and consequently, only the final result will be given herein. The final result has been expressed in terms of dimensionless variables and has been rearranged into a form especially suitable for machine computations:

$$\frac{u}{\bar{u}} = \frac{1 - X^2 + \frac{32}{\pi^3}\sum_{n=1,3,5,\cdots}^{\infty} \frac{(-1)^{\frac{n+1}{2}}}{n^3}\left[\frac{e^{-\frac{n\pi\gamma}{2}(1-Y)} + e^{-\frac{n\pi\gamma}{2}(1+Y)}}{1 + e^{-n\pi\gamma}}\right]\cos\frac{n\pi X}{2}}{\frac{2}{3} - \frac{128}{\gamma\pi^5}\sum_{n=1,3,5,\cdots}^{\infty}\frac{1}{n^5}\left(\frac{1 - e^{-n\pi\gamma}}{1 + e^{-n\pi\gamma}}\right)} \tag{2}$$

Energy Equation

When energy conservation is applied for steady heat transfer to flow with constant fluid properties and no viscous dissipation, the governing differential equation is

$$\rho c_p u \frac{\partial T}{\partial z} = k\left(\frac{\partial^2 T}{\partial x^2} + \frac{\partial^2 T}{\partial y^2} + \frac{\partial^2 T}{\partial z^2}\right) \tag{3}$$

Equation (3) is further simplified by the additional conditions imposed on the problem. Under the assumptions of constant heating per unit length and fully developed temperature profiles, an overall heat balance leads to the result that the axial temperature gradient is constant, that is,

$$\frac{\partial T}{\partial z} = \frac{Q}{\rho c_p \bar{u} 4ab}, \quad \frac{\partial^2 T}{\partial z^2} = 0$$

Substituting into equation (3) yields

$$\frac{u}{\bar{u}}\frac{Q}{4ab} = k\left(\frac{\partial^2 T}{\partial x^2} + \frac{\partial^2 T}{\partial y^2}\right) \tag{4}$$

Equation (4), with the velocity distribution equation (2) substituted into

it, is to be solved subject to the appropriate boundary conditions. Since the velocity and temperature distributions are symmetrical about both center planes ($x = 0$, $y = 0$), only one quarter of the cross section need be treated with symmetry imposed along the centerlines. Along the broad sides a heat flux is imposed between $y = \pm c$, and the remainder of the broad sides and the short sides are assumed to be perfectly insulated. The heat-flux variation in the fueled region is assumed to be of the form

$$q = \frac{Q}{4c\left(1 - \frac{2P}{\pi}\right)}\left(1 - P \cos \frac{y\pi}{2c}\right) \tag{5}$$

where P is a positive constant. The q varies from its lowest value at the center of the broad side ($y = 0$) to its maximum at $y = c$, which is at the edge of the fuel loading. Equation (5) has been arranged so that Q is the total heat input per unit length of channel, that is,

$$Q = 4 \int_0^c q \, dy$$

When $P = 0$ we have the limiting case of uniform heat flux in the fueled region so that $Q = 4cq$. For the results given in the section DISCUSSION OF RESULTS the total heat input per unit channel length Q is always held constant; consequently, as the width c of the fuel is decreased, the local q has to be proportionately increased. The boundary conditions for a quarter of the cross section can be summarized as

$$\left.\begin{aligned}
&\frac{\partial T}{\partial y} = 0 && y = 0,b;\ 0 \le x \le a \\
&\frac{\partial T}{\partial x} = 0 && x = 0;\ 0 \le y \le b \\
&\frac{\partial T}{\partial x} = \frac{Q\left(1 - P \cos \frac{y\pi}{2c}\right)}{4ck\left(1 - \frac{2P}{\pi}\right)} && x = a;\ 0 \le y \le c \\
&\frac{\partial T}{\partial x} = 0 && x = a;\ c < y \le b
\end{aligned}\right\} \tag{6}$$

As shown by Cheng (ref. 3), the analytical solution of equation (4) becomes quite involved, even when the simpler boundary condition of uniform heating around the periphery is imposed. The present condition, which has a discontinuity in wall heating along the broad side at the edge of the fueled region, adds additional complexity; and, hence, it was decided to use a combined numerical and analytical solution procedure.

Superposition of Solutions

The energy equation (4) is written in terms of the dimensionless temperature θ

$$\nabla^2\theta = \frac{\partial^2\theta}{\partial x^2} + \frac{\partial^2\theta}{\partial y^2} = \frac{1}{ab}\,\frac{u}{\bar{u}} \tag{4a}$$

Let θ be composed of two solutions

$$\theta = \theta_P + \theta_L \tag{7}$$

where θ_P satisfies the Poisson equation

$$\nabla^2\theta_P = \frac{1}{ab}\,\frac{u}{\bar{u}} \tag{8}$$

and θ_L satisfies the Laplace equation

$$\nabla^2\theta_L = 0 \tag{9}$$

The boundary conditions for equations (8) and (9) have to be specified. Since equation (8) contains the convective term $\frac{1}{ab}\,\frac{u}{\bar{u}}$, the heat addition for the θ_P solution will have to equal the total heat input to the channel. This is accomplished by imposing a uniform heat addition $q = \frac{Q}{4b}$ over the entire width of the broad sides. The short sides are left insulated. The boundary conditions for θ_P are then

$$\left.\begin{aligned} \frac{\partial\theta_P}{\partial y} &= 0 && y = 0,b;\ 0 \le x \le a \\ \frac{\partial\theta_P}{\partial x} &= 0 && x = 0;\ 0 \le y \le b \\ \frac{\partial\theta_P}{\partial x} &= \frac{1}{b} && x = a;\ 0 \le y \le b \end{aligned}\right\} \tag{8a}$$

The conditions on θ_L must be such that when they are added to equations (8a) the conditions in equations (6) are obtained. Hence, for θ_L we have

$$\left.\begin{aligned}
&\frac{\partial \theta_L}{\partial y} = 0 && y = 0,b;\ 0 \le x \le a \\
&\frac{\partial \theta_L}{\partial x} = 0 && x = 0;\ 0 \le y \le b \\
&\frac{\partial \theta_L}{\partial x} = -\frac{1}{b} + \frac{1 - P\cos\frac{y\pi}{2c}}{c\left(1 - \frac{2P}{\pi}\right)} && x = a;\ 0 \le y \le c \\
&\frac{\partial \theta_L}{\partial x} = -\frac{1}{b} && x = a;\ c < y \le b
\end{aligned}\right\} \qquad (9a)$$

Since equation (9) does not contain a convective term, the net heat addition through the broad walls as specified by (9a) must be zero, as is shown by computing the total heat addition along the boundary $x = a$:

$$c\left(-\frac{1}{b}\right) + \frac{\int_0^c \left(1 - P\cos\frac{y\pi}{2c}\right)dy}{c\left(1 - \frac{2P}{\pi}\right)} + (b - c)\left(-\frac{1}{b}\right) = 0$$

Hence, the solution to equations (4a) and (6) has been reduced to the sum of a simpler forced convection solution with uniform heating on the broad walls (Poisson's eq. (8)) and a pure conduction solution (Laplace's eq. (9)) with conditions (eq. (9a)) imposed. This method of solution is valid for any arbitrary wall heat flux distribution. For each aspect ratio γ only one Poisson temperature distribution is needed, and to this is added a solution of Laplace's equation to account for each heat flux variation.

Solution for θ_P

The solution for θ_P could be obtained analytically in a manner similar to the one used in reference 3. However, the form of the solution becomes quite involved; and, hence, it was decided to use a numerical procedure for this part of the problem. The energy equation was expressed in finite difference form, which led to a matrix of unknown temperatures at points distributed over the channel cross section. The matrix was solved with an IBM 704 computer by using an implicit line iteration technique. The details of the numerical procedure are given in the appendix. This procedure can also be used to solve the original problem directly because the conditions in equations (6) are only very slightly more complicated than those in equations (8a). Some complete solutions were obtained numerically to serve as a check on the superposition results. The solution for θ_P can also be obtained approximately by a variational method as shown in reference 2, where results are given for an aspect

ratio of 10. Because the θ_P solutions form a basis for the superposition method that can be applied to problems of arbitrary heat flux, the $\theta_P - \theta_{P,b}$ values are given in table I.

TABLE I. - DIMENSIONLESS TEMPERATURE DISTRIBUTIONS FOR UNIFORM HEATING OVER ENTIRE WIDTH OF BROAD SIDES

(a) Aspect ratio, b/a, 10

Dimensionless short-side coordinate, X = x/a	Dimensionless temperature, $\theta_P - \theta_{P,b}$; Dimensionless long-side coordinate, Y = y/b													
	0	0.1	0.2	0.3	0.4	0.5	0.6	0.7	0.8	0.9	0.94	0.96	0.98	1.00
0.0	-0.111	-0.108	-0.0989	-0.0827	-0.0591	-0.0281	0.00861	0.0513	0.101	0.152	0.170	0.178	0.183	0.185
.1	-.111	-.108	-.0981	-.0819	-.0583	-.0274	.00928	.0520	.102	.153	.171	.179	.184	.186
.2	-.108	-.105	-.0959	-.0796	-.0561	-.0251	.0116	.0543	.104	.155	.173	.180	.186	.188
.3	-.105	-.102	-.0921	-.0759	-.0523	-.0213	.0153	.0580	.107	.158	.176	.183	.186	.191
.4	-.0995	-.0964	-.0870	-.0708	-.0472	-.0162	.0204	.0631	.112	.163	.181	.188	.193	.195
.5	-.0931	-.0900	-.0806	-.0644	-.0408	-.00980	.0268	.0695	.119	.169	.186	.193	.198	.200
.6	-.0856	-.0825	-.0730	-.0568	-.0332	-.00226	.0344	.0770	.126	.176	.193	.199	.204	.206
.7	-.0771	-.0740	-.0645	-.0483	-.0247	+.00624	.0429	.0855	.134	.184	.200	.207	.211	.213
.8	-.0679	-.0647	-.0553	-.0391	-.0155	+.0155	.0521	.0947	.143	.193	.209	.215	.219	.221
.9	-.0581	-.0550	-.0455	-.0293	-.00575	+.0252	.0618	.104	.153	.202	.218	.224	.228	.230
.94	-.0541	-.0510	-.0416	-.0254	-.00177	+.0292	.0658	.108	.157	.206	.222	.228	.232	.233
.96	-.0521	-.0490	-.0396	-.0234	+.000230	+.0312	.0678	.110	.159	.208	.224	.230	.234	.235
.98	-.0501	-.0470	-.0376	-.0214	+.00225	+.0332	.0698	.112	.161	.210	.226	.232	.236	.237
1.00	-.0481	-.0450	-.0356	-.0194	+.00423	+.0352	.0718	.114	.163	.212	.228	.234	.238	.239

(b) Aspect ratio, b/a, 20

Dimensionless short-side coordinate, X = x/a	Dimensionless temperature, $\theta_P - \theta_{P,b}$; Dimensionless long-side coordinate, Y = y/b													
	0	0.1	0.2	0.3	0.4	0.5	0.6	0.7	0.8	0.9	0.94	0.96	0.98	1.00
0.0	-0.112	-0.109	-0.0987	-0.0818	-0.0582	-0.0279	0.00910	0.0529	0.103	0.160	0.183	0.194	0.202	0.207
.1	-.112	-.108	-.0983	-.0814	-.0579	-.0276	.00945	.0533	.104	.160	.183	.194	.203	.207
.2	-.111	-.107	-.0971	-.0803	-.0567	-.0264	.0106	.0544	.105	.161	.184	.195	.204	.208
.3	-.109	-.106	-.0953	-.0785	-.0549	-.0246	.0124	.0562	.107	.163	.186	.197	.205	.209
.4	-.106	-.103	-.0928	-.0759	-.0523	-.0220	.0150	.0586	.109	.166	.189	.199	.207	.211
.5	-.103	-.0997	-.0896	-.0727	-.0492	-.0189	.0182	.0620	.112	.169	.192	.202	.210	.214
.6	-.0993	-.0959	-.0858	-.0690	-.0454	-.0151	.0219	.0657	.116	.173	.195	.205	.213	.217
.7	-.0951	-.0917	-.0816	-.0648	-.0412	-.0109	.0261	.0695	.120	.177	.199	.209	.217	.220
.8	-.0905	-.0871	-.0770	-.0602	-.0366	-.00632	.0307	.0741	.125	.181	.204	.213	.221	.224
.9	-.0856	-.0823	-.0722	-.0553	-.0318	-.00146	.0356	.0794	.130	.186	.208	.216	.225	.229
.94	-.0837	-.0803	-.0702	-.0534	-.0298	+.000525	.0376	.0813	.132	.188	.210	.220	.227	.231
.96	-.0827	-.0793	-.0692	-.0524	-.0288	+.00152	.0386	.0823	.133	.189	.211	.221	.228	.232
.98	-.0817	-.0783	-.0682	-.0514	-.0278	+.00252	.0396	.0833	.134	.190	.212	.222	.229	.233
1.00	-.0807	-.0773	-.0672	-.0504	-.0268	+.00352	.0405	.0843	.135	.191	.213	.223	.230	.234

Solution for θ_L

The solution for θ_L was found analytically by using a product solution of the form

$$\theta_L = \sum_{m=1,2,3,\cdots}^{\infty} A_m \cos\left(\frac{m\pi}{b} y\right)\cosh\left(\frac{m\pi}{b} x\right) \tag{10}$$

This equation already satisfies the zero derivative boundary conditions in the first two lines of equations (9a). To satisfy the conditions at $x = a$ equation (10) is differentiated and evaluated at $x = a$

$$\left.\frac{\partial\theta_L}{\partial x}\right|_{x=a} = \sum_{m=1,2,3,\cdots}^{\infty} A_m\left(\frac{m\pi}{b}\right)\cos\left(\frac{m\pi y}{b}\right)\sinh\left(\frac{m\pi a}{b}\right) \tag{11}$$

To obtain the coefficients A_m, the boundary condition is expanded in a Fourier series. This expansion gives

$$\int_0^b \cos\left(\frac{m\pi y}{b}\right)\left(\frac{\partial\theta_L}{\partial x}\right)_{x=a} dy = \int_0^b A_m \frac{m\pi}{b} \cos^2\left(\frac{m\pi y}{b}\right)\sinh\left(\frac{m\pi a}{b}\right)dy \tag{12}$$

Substituting for $(\partial\theta_L/\partial x)_{x=a}$ results in

$$\int_0^c \left[-\frac{1}{b} + \frac{1 - P\cos\left(\frac{y\pi}{2c}\right)}{c\left(1 - \frac{2P}{\pi}\right)}\right]\cos\left(\frac{m\pi y}{b}\right)dy + \int_c^b \left(-\frac{1}{b}\right)\cos\left(\frac{m\pi y}{b}\right)dy$$

$$= A_m\left(\frac{m\pi}{b}\right)\sinh\left(\frac{m\pi a}{b}\right)\int_0^b \cos^2\left(\frac{m\pi y}{b}\right)dy$$

which yields

$$A_m = \frac{2\left\{\left(\frac{b}{m\pi}\right)\sin\left(\frac{m\pi c}{b}\right) - P\left[\frac{\sin\left(\frac{1}{2} - \frac{mc}{b}\right)\pi}{2\pi\left(\frac{1}{2c} - \frac{m}{b}\right)} + \frac{\sin\pi\left(\frac{1}{2} + \frac{mc}{b}\right)}{2\pi\left(\frac{1}{2c} + \frac{m}{b}\right)}\right]\right\}}{m\pi c\left(1 - \frac{2D}{\pi}\right)\sinh\left(\frac{m\pi a}{b}\right)} \tag{13}$$

Equation (13) is inserted into equation (10) to obtain θ_L.

Bulk Temperature

After the solution for θ has been found, the bulk temperature θ_b is computed so that the results can be presented in the general dimensionless form $\theta - \theta_b$. The bulk temperature is found from the definition

$$\theta_b = \frac{1}{ab}\int_0^a \int_0^b \frac{u}{\bar{u}}\,\theta\,dx\,dy \tag{14}$$

From the superposition of solutions θ is given by $\theta = \theta_P + \theta_L$, and after this is substituted into equation (14), $\theta_b = \theta_{P,b} + \theta_{L,b}$ is obtained. Then the desired solution can be written as

$$\theta - \theta_b = (\theta_P - \theta_{P,b}) + (\theta_L - \theta_{L,b}) \tag{15}$$

The values of $\theta_{P,b}$ were obtained numerically, and values of $\theta_P - \theta_{P,b}$ are

given in table I. The value of $\theta_{L,b}$ remains to be computed, which could be done by substituting equations (2) and (10) into equation (14) and carrying out the integration, but a much simpler procedure is as follows. Equation (8) is solved for $u/\bar{u}$ and substituted into equation (14). The bulk temperature can then be written as

$$\theta_{L,b} = \iint_R \theta_L \nabla^2 \theta_P \, dx \, dy \tag{16}$$

By using the second form of Green's theorem, equation (16) can be converted to

$$\theta_{L,b} = \int_\Gamma \left(\theta_L \frac{\partial \theta_P}{\partial \nu} - \theta_P \frac{\partial \theta_L}{\partial \nu} \right) ds + \iint_R \theta_P \nabla^2 \theta_L \, dA \tag{17}$$

where the quantities $\partial\theta_P/\partial\nu$ and $\partial\theta_L/\partial\nu$ are the normal derivatives of θ_P and θ_L and are known over the boundary Γ from equations (8a) and (9a).

Since $\nabla^2\theta_L = 0$ over the region R, the second integral is zero. Then

$$\theta_{L,b} = \frac{1}{b} \int_0^b \theta_L(a,y)dy - \int_0^c \left[-\frac{1}{b} + \frac{1 - P\cos\left(\frac{y\pi}{2c}\right)}{c\left(1 - \frac{2P}{\pi}\right)} \right] \theta_P(a,y)dy$$

$$+ \frac{1}{b} \int_c^b \theta_P(a,y)dy \tag{18}$$

The first integral is identically zero because of the cosine variation that θ_L has in the y-direction (eq. (10)). It was noted on page 9 that

$$- \int_0^c \left[-\frac{1}{b} + \frac{1 - P\cos\left(\frac{y\pi}{2c}\right)}{c\left(1 - \frac{2P}{\pi}\right)} \right] dy + \frac{1}{b} \int_c^b dy = 0$$

Because of this relation a constant $(-\theta_{P,b})$ can be added to θ_P in equation (18). Then $\theta_{L,b}$ can be written as

$$\theta_{L,b} = \frac{1}{b}\int_0^b \left[\theta_P(a,y) - \theta_{P,b}\right]dy$$

$$- \int_0^c \left[\frac{1 - P\cos\left(\frac{y\pi}{2c}\right)}{c\left(1 - \frac{2P}{\pi}\right)}\right]\left[\theta_P(a,y) - \theta_{P,b}\right]dy \qquad (19a)$$

For the special case when $P = 0$ (i.e., uniform heating in the fueled region), equation (19a) simplifies to

$$\theta_{L,b} = \frac{1}{b}\int_0^b \left[\theta_P(a,y) - \theta_{P,b}\right]dy - \frac{1}{c}\int_0^c \left[\theta_P(a,y) - \theta_{P,b}\right]dy \qquad (19b)$$

or in dimensionless form

$$\theta_{L,b} = \int_0^1 \left[\theta_P(1,Y) - \theta_{P,b}\right]dY - \frac{b}{c}\int_0^{c/b} \left[\theta_P(1,Y) - \theta_{P,b}\right]dY \qquad (19c)$$

Thus, from equations (19) the $\theta_{L,b}$ can be easily evaluated from the values of $\theta_P - \theta_{P,b}$ along the boundary.

Variational Solution

As mentioned before, an approximate solution for $\theta_P - \theta_{P,b}$ has been given in reference 2 for $\gamma = 10$. This solution can be combined with equation (10) to provide an approximate closed-form analytical solution. The expression for θ_P from reference 2 is

$$\theta_P - \theta_{P,b} = \frac{1}{11}\left[\frac{11\,X^2}{20} - 0.11703(X^2 - 1)^2 - 10.291(Y^2 - 1)^2\right.$$

$$\left. - 0.038328(X^2 - 1)^2(Y^2 - 1)^2 - 12.05(Y^2 - 1)^3 - 4.9697(Y^2 - 1)^4\right] \qquad (20)$$

Equation (20) can be inserted into equation (19) to determine $\theta_{L,b}$ for a given c/b and then combined with equation (10) to yield the solution in equation (15).

Numerical results were carried out for two aspect ratios, 10 and 20. The important parameter in the problem is the distance between the edge of the fuel loading and the corner, d = b - c; this distance can be expressed in terms of the channel spacing as d/2a. This parameter was varied in the range from 0 to 0.5 for γ = 10 and 20. Results are given for both a uniform heat flux along the heated region and for a cosine variation with P = 0.20.

DISCUSSION OF RESULTS

In figures 3 and 4 are shown the wall temperature distributions for various widths of the unheated areas between the edges of the fuel loading on the broad sides and the corners. The figures are for two aspect ratios, 10 and 20. The wall temperature variable that has been plotted is nondimensionalized with respect to Q, the heat input to the channel per unit length in the flow direction. Hence, when the different curves in figures 3 and 4 are being compared, they are for the same total heat addition over the channel cross section. The curves begin at the center of the heated side, extend across to the corner, and then extend down to the center of the unheated short side.

When the broad sides are completely heated (d/2a = 0, c/b = 1), the wall temperature is a maximum at the corner. In the corner region the flow velocities are low; hence, the imposed wall heat flux cannot be removed by convection as easily as in the regions away from the corners, where the convective velocities are much higher. As a result, the corner wall temperature rises to com-

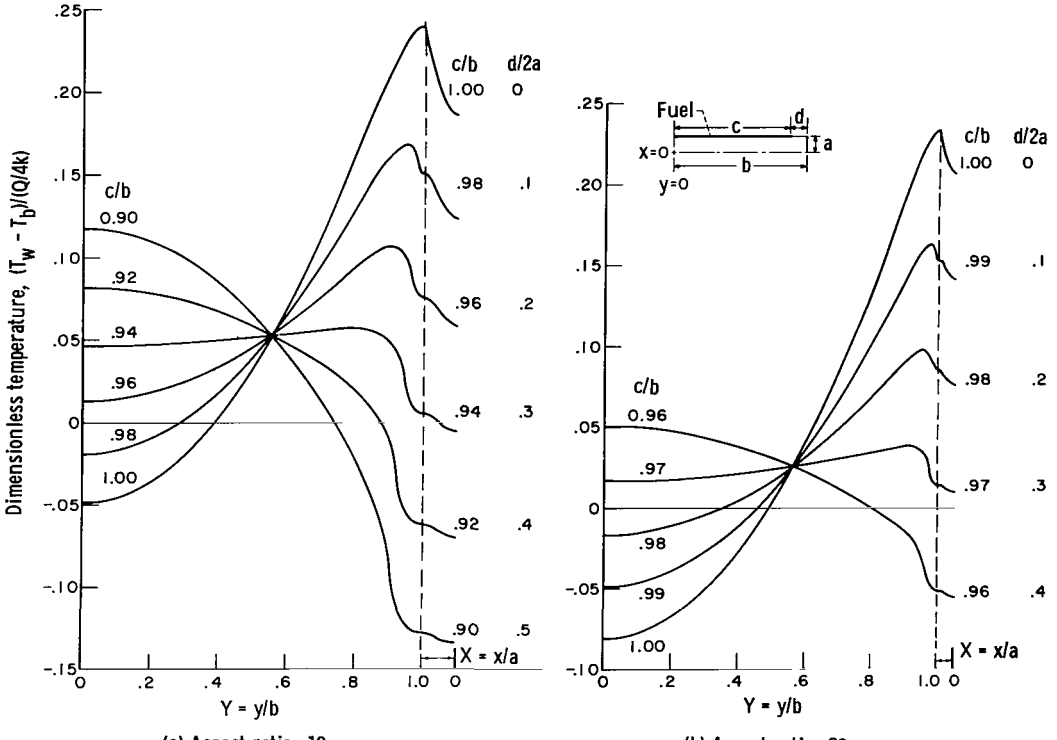

(a) Aspect ratio, 10. (b) Aspect ratio, 20.

Figure 3. - Wall temperature distribution for uniform heating in fueled region.

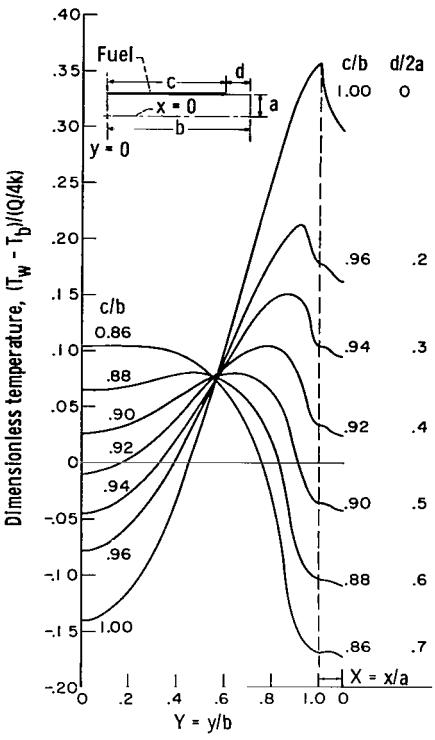

Figure 4. - Wall temperature distribution with cosine heat flux distribution in fueled region. Amplitude P, 0.2; aspect ratio, 10.

pensate for the poor convection, and this temperature increase enables the heat to diffuse toward a region of better convection.

For uniform heating over the entire broad sides, figure 3 indicates that the aspect ratio has a relatively small influence on the wall temperature distributions and the magnitude of the peak temperature. The insensitivity of the peak temperature to γ is possibly due to two compensating influences. For ducts of high aspect ratio, the low-velocity regions adjacent to the side walls occupy only a small fraction of the total cross section, and this fraction decreases as γ is increased. Consequently, the peak temperature tends to decrease because a smaller portion of the total heat input has to be diffused away from the low-velocity region. As γ increases, however, there is an increase in the heat-flow resistance for this diffusion in the direction along the broad walls, and this resistance tends to increase the peak temperature. As a result, the peak temperature remains almost constant in the range of large γ considered here.

The most significant result is the sizeable influence exerted on the wall temperature distribution by small changes in the location of the fuel loading. As the edge of the heated region is moved away from the corner, the fluid in the region near the short side walls receives less energy directly from the broad walls. This fluid serves as a heat sink that helps carry away some of the energy from the adjacent heated fluid region. From figure 3 it is evident that only a small unheated region is necessary to form a sufficiently large heat sink to shift the maximum wall temperature to the center of the broad side. When the fueled region is uniformly heated, for both $\gamma = 10$ and 20 the temperature along most of the broad side is very nearly constant when there is an intermediate spacing of $d/2a = 0.3$ between the heated area and the corner.

When the heating in the fueled region varies in a cosine fashion with a local heat flux that is increasing toward the corner, the temperature variations become more pronounced as shown in figure 4. These results are for an aspect ratio of 10 and a heat flux at the edge of the fuel loading that is 25 percent greater than at the center of the broad side. Because of the increased heating in the corner region, it is necessary to move the fuel farther away from the corner to achieve the most uniform temperature distribution possible. For no value of $d/2a$ does the wall temperature become as nearly constant as for the uniform heating case. The peak temperature appears at the center of the broad side when $d/2a$ is greater than 0.65 instead of 0.35 as was the case with uniform heating in the wall.

Figures 3 and 4 show that at some places along the wall the value of $T_w - T_b$ is negative, that is, T_b is larger than T_w. This negative value may seem to contradict the fact that heat is flowing from the wall to the fluid; however, it must be recalled that T_b is an average value over the entire cross section, while T_w is a local value along the wall. For example, in figure 3(a), for $d/2a = 0$, the fluid is at a high temperature near the side walls; this higher temperature raises the average fluid temperature over the cross section to a value higher than the wall temperature at the center of the broad side. Since figures 3 and 4 do not give any details of the fluid temperature distribution over the cross section, some sample distributions have been given in tables I and II.

Some comments are necessary to relate these results to the problem of fuel-channel design in a reactor. Two assumptions have been made in the analysis, laminar flow and no heat conduction in the channel wall. These assumptions both tend to make the computed temperature variations more extreme than they would usually be in practice. In most cases the flow would be turbulent, which results in a more uniform velocity distribution over the cross section and also produces secondary flows that move cooler fluid from the central core to the corner regions. These factors along with peripheral conduction in the

TABLE II. - DIMENSIONLESS TEMPERATURE DISTRIBUTIONS OVER CHANNEL CROSS SECTION WITH UNIFORM HEATING IN FUELED REGION

(a) Aspect ratio, b/a, 10; dimensionless unheated width on broad side, d/2a, 0.1

Dimensionless short-side coordinate, X = x/a	Dimensionless temperature, $(T_w - T_b)/(Q/4k)$ — Dimensionless long-side coordinate, Y = y/b									
	0	0.2	0.4	0.6	0.8	0.9	0.94	0.96	0.98	1.00
0.0	-0.0831	-0.0735	-0.0451	0.00190	0.0664	0.101	0.113	0.118	0.122	0.123
.2	-.0800	-.0704	-.0420	.00499	.0694	.104	.115	.120	.124	.125
.4	-.0710	-.0614	-.0330	.0140	.0782	.112	.122	.126	.129	.130
.6	-.0568	-.0472	-.0189	.0281	.0921	.124	.133	.136	.137	.138
.8	-.0388	-.0292	-.000866	.0461	.110	.141	.149	.149	.147	.146
.9	-.0289	-.0193	+.00906	.0561	.120	.151	.158	.157	.153	.149
.94	-.0248	-.0152	+.0131	.0601	.124	.155	.161	.161	.155	.150
.96	-.0228	-.0132	+.0151	.0622	.126	.157	.163	.163	.156	.150
.98	-.0208	-.0112	+.0172	.0642	.128	.159	.165	.165	.157	.150
1.00	-.0187	-.00911	+.0192	.0662	.130	.161	.167	.167	.158	.150

(b) Aspect ratio, b/a, 10; dimensionless unheated width on broad side, d/2a, 0.4

Dimensionless short-side coordinate, X = x/a	Dimensionless temperature, $(T_w - T_b)/(Q/4k)$ — Dimensionless long-side coordinate, Y = y/b									
	0	0.2	0.4	0.6	0.8	0.9	0.94	0.96	0.98	1.00
0.0	0.142	0.104	-0.00121	-0.0208	-0.0479	-0.0657	-0.0699	-0.0705	-0.0696	-0.0691
.2	.174	.137	+.00201	-.0176	-.0449	-.0636	-.0684	-.0690	-.0691	-.0686
.4	.268	.231	+.0114	-.00819	-.0356	-.0571	-.0643	-.0664	-.0671	-.0670
.6	.416	.379	+.0262	+.00662	-.0213	-.0465	-.0589	-.0626	-.0643	-.0647
.8	.606	.568	+.0452	+.0256	-.00292	-.0321	-.0529	-.0591	-.0620	-.0627
.9	.711	.673	+.0557	+.0361	+.00710	-.0233	-.0506	-.0579	-.0613	-.0621
.94	.754	.716	+.0600	+.0404	+.0113	-.0194	-.0500	-.0576	-.0612	-.0619
.96	.775	.738	+.0621	+.0425	+.0134	-.0174	-.0498	-.0575	-.0612	-.0618
.98	.797	.760	+.0643	+.0447	+.0155	-.0153	-.0497	-.0575	-.0611	-.0618
1.00	.819	.781	+.0665	+.0469	+.0177	-.0131	-.0496	-.0575	-.0611	-.0618

TABLE II. - Concluded. DIMENSIONLESS TEMPERATURE DISTRIBUTIONS OVER CHANNEL CROSS SECTION WITH UNIFORM HEATING IN FUELED REGION

(c) Aspect ratio, b/a, 20; dimensionless unheated width on broad side, d/2a, 0.1

Dimensionless short-side coordinate, X = x/a	Dimensionless temperature, $(T_w - T_b)/(Q/4k)$ — Dimensionless long-side coordinate, Y = y/b									
	0	0.2	0.4	0.6	0.8	0.9	0.94	0.96	0.98	1.00
0.0	-0.0805	-0.0711	-0.0428	+0.00434	0.0703	0.110	0.126	0.133	0.138	0.142
.2	-.0790	-.0696	-.0413	+.00586	.0719	.111	.127	.134	.139	.142
.4	-.0746	-.0652	-.0369	+.0103	.0763	.116	.131	.138	.142	.145
.6	-.0676	-.0582	-.0299	+.0172	.0832	.122	.137	.144	.147	.148
.8	-.0588	-.0493	-.0210	+.0261	.0921	.131	.146	.152	.154	.151
.9	-.0539	-.0444	-.0161	+.0310	.0970	.136	.151	.156	.158	.153
.94	-.0519	-.0424	-.0141	+.0330	.0990	.138	.153	.158	.160	.153
.96	-.0508	-.0414	-.0131	+.0340	.100	.139	.154	.159	.161	.153
.98	-.0498	-.0404	-.0121	+.0350	.101	.140	.155	.160	.162	.153
1.00	-.0488	-.0394	-.0111	+.0361	.102	.141	.156	.161	.163	.153

(d) Aspect ratio, b/a, 20; dimensionless unheated width on broad side, d/2a, 0.4

Dimensionless short-side coordinate, X = x/a	Dimensionless temperature, $(T_w - T_b)/(Q/4k)$ — Dimensionless long-side coordinate, Y = y/b									
	0	0.2	0.4	0.6	0.8	0.9	0.94	0.96	0.98	1.00
0.0	0.0180	0.0149	0.00533	-0.0106	-0.0330	-0.0470	-0.0533	-0.0557	-0.0563	-0.0550
.2	.0196	.0164	.00688	-.00906	-.0314	-.0455	-.0521	-.0549	-.0558	-.0547
.4	.0241	.0209	.0114	-.00454	-.0269	-.0412	-.0485	-.0524	-.0544	-.0539
.6	.0312	.0281	.0185	+.00259	-.0198	-.0343	-.0427	-.0485	-.0526	-.0528
.8	.0403	.0372	.0276	+.0117	-.0107	-.0253	-.0349	-.0437	-.0507	-.0518
.9	.0453	.0422	.0327	+.0167	-.00565	-.0204	-.0304	-.0410	-.0500	-.0515
.94	.0474	.0443	.0347	+.0188	-.00359	-.0183	-.0284	-.0400	-.0499	-.0515
.96	.0484	.0453	.0358	+.0198	-.00255	-.0173	-.0274	-.0394	-.0498	-.0515
.98	.0495	.0463	.0368	+.0209	-.00151	-.0162	-.0264	-.0389	-.0498	-.0514
1.00	.0505	.0474	.0378	+.0219	-.000473	-.0152	-.0254	-.0384	-.0498	-.0514

walls will tend to reduce the temperature peak in the corner for small d/2a. In most cases the peripheral conduction will be enhanced by the fact that the side walls are thicker than the fuel plates. To ensure that the temperature peaking will be small, the fuel can be moved a short distance away from the corners to a d/2a of about 0.3. There is a danger if d/2a is made too large that the hot spot will be moved to the center of the broad side and may become excessive there.

To summarize, the results have shown that the wall temperature distributions are quite sensitive to the width of the unfueled region d/2a. Even for the limiting case where the flow is laminar and wall conduction is absent, it is only necessary to remove the fuel a very short distance from the corner to avoid temperature peaks there. The preceding conclusion is true even when the heat flux is nonuniform, the maximum near the corner being 25 percent greater than at the plate center.

Lewis Research Center
National Aeronautics and Space Administration
Cleveland, Ohio, May 28, 1964

APPENDIX - NUMERICAL METHOD OF SOLVING THE ENERGY EQUATION

Outlined here is a method for deriving the finite difference equations, their restatement in matrix notation, and the derivation of the overrelaxation factor that gives the most rapid convergence of the iterative process. The use of this overrelaxation method greatly reduces the computational time as compared with more conventional iterative procedures.

The quarter section of the channel cross section is divided by a grid network into N^2 rectangular increments where $\Delta = (\Delta x/a) = (\Delta y/b) = 1/N$ and $n\Delta = (C/b)$. Then a difference equation is derived for each node of the grid, resulting in $(N + 1)^2$ equations in $(N + 1)^2$ unknowns. In this appendix the development of the difference equations is presented for a typical interior point and a point at the center of the heated boundary. The equations for the other nodes are derived in a similar fashion. The discussion is limited to the case where the heating is uniform in the fueled region, but the extension to variable heating is indicated at the end.

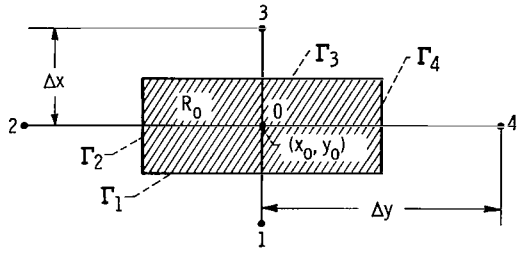

(a) At an interior point.

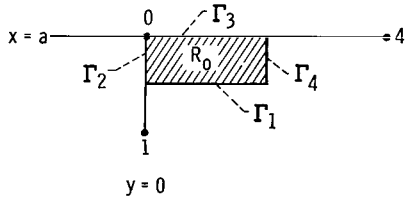

(b) At the center of the heated wall.

Figure 5. - Typical nodes used in derivation of finite-difference equations.

Finite Difference Equations

In figure 5(a), point 0 is an interior node of the mesh with 1, 2, 3, and 4 as neighboring nodes; R_o is the shaded rectangular region associated with point 0. The partial differential equation (4) is integrated over R_o by using Green's Theorem, which states in general

$$\iint_R \nabla^2\theta \, dx \, dy = \int_\Gamma \frac{\partial\theta}{\partial\nu} \, ds \tag{A1}$$

where the right side is the line integral of the normal derivative of θ around the boundary Γ. Substituting equation (4) into equation (A1) gives

$$\frac{1}{ab} \iint_{R_o} \frac{u}{\bar{u}} \, dx \, dy = \sum_{n=1}^{4} \int_{\Gamma_n} \frac{\partial\theta}{\partial\nu} \, ds \tag{A2}$$

Approximating the integrals by

$$\iint_{R_o} \frac{u}{\bar{u}}\, dx\, dy \approx \frac{u_o}{\bar{u}}\, \Delta x\, \Delta y; \quad \int_{\Gamma_1} \frac{\partial\theta}{\partial\nu}\, ds \approx \frac{(\theta_1 - \theta_o)}{\Delta x}\, \Delta y, \text{ etc.}$$

the finite difference analog of equation (A2) can be placed in the form

$$\theta_o = \frac{\gamma^2(\theta_1 + \theta_3) + \theta_2 + \theta_4 - \gamma\Delta^2(u_o/\bar{u})}{2(1 + \gamma^2)} \tag{A3a}$$

In figure 5(b), point 0 is the corner node of the network at the center of the heated region. The procedure just outlined is applied except that the boundary conditions are used on Γ_2 and Γ_3. For uniform heat flux (P = 0) the boundary conditions are

$$\left.\frac{\partial\theta}{\partial\nu}\right|_{\Gamma_2} = 0 \qquad \left.\frac{\partial\theta}{\partial\nu}\right|_{\Gamma_3} = \frac{1}{c}$$

These conditions result in the relation

$$\theta_o = \frac{\frac{\gamma}{n} + \gamma^2\theta_1 + \theta_4}{1 + \gamma^2} \tag{A3b}$$

Matrix Notation

The equations for all the nodes can be written concisely in matrix notation as

$$\Omega\theta = G + U \tag{A4}$$

where Ω is a partitioned matrix of order $(N + 1)^2$

$$\Omega = \begin{pmatrix} A & -B & 0 & \cdot & 0 & 0 \\ -B & 2A & -B & \cdot & 0 & 0 \\ 0 & -B & 2A & \cdot & 0 & 0 \\ \cdot & \cdot & \cdot & \cdot & \cdot & \cdot \\ 0 & 0 & 0 & \cdot & 2A & -B \\ 0 & 0 & 0 & \cdot & -B & A \end{pmatrix} \tag{A5}$$

with submatrices of order $N + 1$

$$A = \begin{pmatrix} (\gamma^2 + 1) & -\gamma^2 & 0 & \cdot & 0 & 0 \\ -\gamma^2 & 2(\gamma^2 + 1) & -\gamma^2 & \cdot & 0 & 0 \\ 0 & -\gamma^2 & 2(\gamma^2 + 1) & \cdot & 0 & 0 \\ \cdot & \cdot & \cdot & \cdot & \cdot & \cdot \\ 0 & 0 & 0 & \cdot & 2(\gamma^2 + 1) & -\gamma^2 \\ 0 & 0 & 0 & \cdot & -\gamma^2 & (\gamma^2 + 1) \end{pmatrix} \tag{A5a}$$

$$B = \text{diag}\ (1,\ 2,\ 2,\ \cdots,\ 2,\ 1) \tag{A5b}$$

The components in G arise from the boundary conditions such as the term γ/n in equation (A3b), while the terms in U come from the left side of equation (4), which gives terms such as $\gamma\ \Delta^2 u_o/\overline{u}$ in equation (A3a). The terms G and U are partitioned conformably with Ω, which gives

$$G = \begin{pmatrix} g_1 \\ g_2 \\ \cdots \\ g_{N+1} \end{pmatrix} \qquad U = \begin{pmatrix} u_1 \\ u_2 \\ \cdots \\ u_{N+1} \end{pmatrix} \tag{A6}$$

where g_i and u_i are $(N + 1) \times 1$ and are given as follows:

$$\left.\begin{aligned} g_1 = g_{n+1} &= \begin{pmatrix} \gamma/n \\ 0 \\ \cdots \\ 0 \end{pmatrix} \\ g_i &= 2g_1 \qquad 2 \le i \le n \\ g_i &= \begin{pmatrix} 0 \\ 0 \\ \cdots \\ 0 \end{pmatrix} \qquad i > n + 1 \end{aligned}\right\} \tag{A7a}$$

$$
\left.
\begin{aligned}
u_1 &= -\Delta^2\gamma \begin{pmatrix} 0 \\ u[N\,\Delta,0]/\bar{u} \\ u[(N-1)\Delta,0]/\bar{u} \\ \cdot\ \cdot\ \cdot\ \cdot\ \cdot\ \cdot\ \cdot\ \cdot \\ u[\Delta,0]/\bar{u} \\ \tfrac{1}{2}\,u[0,0]/\bar{u} \end{pmatrix} \\
u_i &= -2\,\Delta^2\gamma \begin{pmatrix} 0 \\ u[N\,\Delta,(i-1)\Delta]/\bar{u} \\ u[N-1)\Delta,(i-1)\Delta]/\bar{u} \\ \cdot\ \cdot\ \cdot\ \cdot\ \cdot\ \cdot\ \cdot\ \cdot\ \cdot\ \cdot\ \cdot \\ u[\Delta,(i-1)\Delta]/\bar{u} \\ \tfrac{1}{2}\,u[0,(i-1)\Delta]/\bar{u} \end{pmatrix} \qquad 2 \le i \le N \\
u_{N+1} &= \underline{0}
\end{aligned}
\right\} \qquad \text{(A7b)}
$$

The matrix Ω receives its particular form by numbering the mesh points from top to bottom in columns starting with the first column at the left of the rectangle.

Iterative Procedure

For the iterative procedure it is necessary to decompose Ω as follows:

$$\Omega = \mathscr{A} - \mathscr{B} - \mathscr{B}^T \qquad \text{(A8)}$$

(the superscript T denoting transpose) where

$$\mathscr{A} = \text{diag}(A,\ 2A,\ \cdot\ \cdot\ \cdot,\ 2A,\ A) \qquad \text{(A9a)}$$

and

$$\mathcal{B} = \begin{pmatrix} 0 & 0 & 0 & \cdot & 0 & 0 & 0 \\ B & 0 & 0 & \cdot & 0 & 0 & 0 \\ 0 & B & 0 & \cdot & 0 & 0 & 0 \\ \cdot & \cdot & \cdot & \cdot & \cdot & \cdot & \cdot \\ 0 & 0 & 0 & \cdot & 0 & 0 & 0 \\ 0 & 0 & 0 & \cdot & B & 0 & 0 \\ 0 & 0 & 0 & \cdot & 0 & B & 0 \end{pmatrix} \tag{A9b}$$

The iterative scheme is defined by

$$\mathcal{A}\underline{\theta}^{(m+1)} = \omega\left[\mathcal{B}\underline{\theta}^{(m+1)} + \mathcal{B}^{T}\underline{\theta}^{(m)} + G + U\right] + (1 - \omega)\mathcal{A}\underline{\theta}^{(m)} \tag{A10}$$

which is applied as follows:

($\underline{\theta}^{(o)}$ is an initial guess), (1) $G + U$ and $\underline{\theta}^{(m)}$, the m^{th} iterate for $\underline{\theta}$ at all the mesh points are given.

(2) W is computed from $\mathcal{A}W = \mathcal{B}\underline{\theta}^{(m+1)} + \mathcal{B}^{T}\underline{\theta}^{(m)} + G + U$.

(3) Then $\underline{\theta}^{(m+1)} = \omega W + (1 - \omega)\underline{\theta}^{(m)}$.

The appearance of $\underline{\theta}^{(m+1)}$ in the right side of the equation in step (2) causes no difficulty since $\mathcal{B}$ is strictly lower triangular by blocks. The iteration is carried out one column after the other from left to right, each column of $\underline{\theta}$'s being computed simultaneously; hence, this iteration process is called the line method.

Overrelaxation Factor

The value of ω giving the fastest convergence of the iterative process is usually given by

$$\omega_b = \frac{2}{1 + \sqrt{1 - \rho^2}} \tag{A11}$$

where $C = \mathcal{A}^{-1}(\mathcal{B} + \mathcal{B}^{T})$ and $\rho = \rho(C)$ is the spectral radius of C (ref. 8). In the present case, however, C has eigenvalues ± 1 so that the iterative process would fail to converge for ω calculated from $\rho(C)$.

The occurrence of the eigenvalue $+1$ is a result of the fact that solutions of Neumann problems are determined only up to an additive constant. The value -1 was introduced by the decomposition of Ω. Since C is two-cyclic (ref. 9),

deflation of C by the eigenvalues ± 1 yields a matrix C' that is again two-cyclic and to which the Young-Frankel theory of successive overrelaxation may be applied.

If $\lambda_1, \lambda_2, \lambda_3, \cdots$ are the eigenvalues of C,

$$1 = |\lambda_1| = |\lambda_2| > |\lambda_3| = |\lambda_4| > |\lambda_5| \cdots$$

Then $0, 0, \lambda_3, \lambda_4, \cdots$ are the eigenvalues of C'. Let $V_1, V_2, \cdots$ be the associated eigenvectors, that is, $CV_i = \lambda_i V_i$. Components of the error may be ignored along V_1, since this may be regarded as the additive constant referred to previously; components of the error may be ignored along V_2 also since averaging $\underline{\theta}^{(m)}$ with $C\underline{\theta}^{(m)}$ will eliminate this error. The computation of ω_b, therefore, is based upon λ_3; that is,

$$\omega_b = \frac{2}{1 + \sqrt{1 - |\lambda_3|^2}}$$

The eigenvalues of C are given by

$$\frac{\cos \frac{(\kappa - 1)\pi}{N}}{\gamma^2 \left[\cos \frac{(j - 1)\pi}{N} - 1\right] - 1} \qquad \kappa, j = 1, \cdots, N + 1$$

if N is sufficiently large, $\lambda_3 = \cos(\pi/N)$ and

$$\omega_b = \frac{2}{1 + \sin(\pi/N)}$$

Numerical experiments verified the optimum character of this number.

Remarks

Early in the solution it was noticed that the residuals (e.g., for eq. (A3b) the residual is defined to be $\theta_o - \frac{\frac{\gamma}{n} + \gamma^2\theta_1 + \theta_4}{1 + \gamma^2}$) after several iterations achieved a constant value throughout the mesh and remained at that value for every iteration thereafter; however, the value of $\underline{\theta}^{(m)}$ kept increasing. The reason for the drifting was that the $\bar{u}$ used to normalize the u at each node was evaluated by using the series in the denominator of equation (2), which is obtained from an analytical integration of the velocity over the cross section. The use of the series form of $\bar{u}$ introduces an inconsistency in the system of equations (A4) in which integrals have been approximated by the trapezoidal rule; hence, by using the trapezoidal rule to evaluate $\bar{u}$, the drifting was eliminated.

When passing from the constant heat flux case to the cosine variation, the boundary condition corresponding to equation (5) must be written by using the trapezoidal rule to compute the normalizing factor in the denominator, that is,

$$\frac{\partial\theta}{\partial x} = \frac{1 - P\cos\frac{y\pi}{2c}}{c\left(1 - \frac{P}{2n}\cot\frac{\pi}{4n}\right)} \qquad x = a,\ 0 \le y \le c$$

whose limit as Δ approaches 0 is the boundary condition in equations (6).

REFERENCES

1. Levy, S., Fuller, R. A., and Niemi, R. O.: Heat Transfer to Water in Thin Rectangular Channels. Jour. Heat Transfer (Trans. ASME), ser. C, vol. 81, no. 2, May 1959, pp. 129-140; discussion, pp. 141-143.

2. Sparrow, E. M., and Siegel, R.: A Variational Method for Fully Developed Laminar Heat Transfer in Ducts. Jour. Heat Transfer (Trans. ASME), ser. C, vol. 81, no. 2, May 1959, pp. 157-164.

3. Cheng, H. M.: Analytical Investigation of Fully Developed Laminar Flow Forced Convection Heat Transfer in Rectangular Ducts with Uniform Heat Flux. M.S. Thesis, M.I.T., 1957.

4. Eckert, E. R. G., and Irvine, T. F., Jr.: Flow in Corners of Passages with Noncircular Cross Sections. Trans. ASME, vol. 78, no. 4, May 1956, pp. 709-718.

5. Eckert, E. R. G., and Irvine, T. F., Jr.: Pressure Drop and Heat Transfer in a Duct with Triangular Cross Section. Jour. Heat Transfer (Trans. ASME), ser. C, vol. 82, no. 2, May 1960, pp. 125-138.

6. Eckert, E. R. G., Irvine, T. F., Jr., and Yen, J. T.: Local Laminar Heat Transfer in Wedge-Shaped Passages. Trans. ASME, vol. 80, no. 7, Oct. 1958, pp. 1433-1438.

7. Knudsen, J. G., and Katz, D. L.: Fluid Dynamics and Heat Transfer. McGraw-Hill Book Co., Inc., 1958.

8. Forsythe, G. E., and Wasow, W. R.: The Young-Frankel Theory of Successive Overrelaxation. Sec. 22-1, Finite-Difference Methods for Partial Differential Equations, John Wiley & Sons, Inc., 1960.

9. Varga, Richard S.: p-Cyclic Matrices: A Generalization of the Young-Frankel Successive Overrelaxation Scheme. Pacific Jour. Math., vol. 9, 1959, pp. 617-628.

2/1/85

"The aeronautical and space activities of the United States shall be conducted so as to contribute . . . to the expansion of human knowledge of phenomena in the atmosphere and space. The Administration shall provide for the widest practicable and appropriate dissemination of information concerning its activities and the results thereof."

—NATIONAL AERONAUTICS AND SPACE ACT OF 1958

NASA SCIENTIFIC AND TECHNICAL PUBLICATIONS

TECHNICAL REPORTS: Scientific and technical information considered important, complete, and a lasting contribution to existing knowledge.

TECHNICAL NOTES: Information less broad in scope but nevertheless of importance as a contribution to existing knowledge.

TECHNICAL MEMORANDUMS: Information receiving limited distribution because of preliminary data, security classification, or other reasons.

CONTRACTOR REPORTS: Technical information generated in connection with a NASA contract or grant and released under NASA auspices.

TECHNICAL TRANSLATIONS: Information published in a foreign language considered to merit NASA distribution in English.

TECHNICAL REPRINTS: Information derived from NASA activities and initially published in the form of journal articles.

SPECIAL PUBLICATIONS: Information derived from or of value to NASA activities but not necessarily reporting the results of individual NASA-programmed scientific efforts. Publications include conference proceedings, monographs, data compilations, handbooks, sourcebooks, and special bibliographies.

Details on the availability of these publications may be obtained from:

SCIENTIFIC AND TECHNICAL INFORMATION DIVISION

NATIONAL AERONAUTICS AND SPACE ADMINISTRATION

Washington, D.C. 20546